Nanomaterials and Nanotechnology

OPEN ACCESS
ARTICLE

# Synthesis of Nitrogen-Doped Carbon Nanocoils with Adjustable Morphology using Ni–Fe Layered Double Hydroxides as Catalyst Precursors

Regular Paper

Tomohiro Iwasaki[1*], Masashi Tomisawa[1], Takuma Yoshimura[1], Hideya Nakamura[1], Masao Ohyama[2], Katsuya Asao[2] and Satoru Watano[1]

1 Department of Chemical Engineering, Osaka Prefecture University, Osaka, Japan
2 Technology Research Institute of Osaka Prefecture, Osaka, Japan
* Corresponding author(s) E-mail: iwasaki@chemeng.osakafu-u.ac.jp

Received 14 August 2014; Accepted 03 December 2014

DOI: 10.5772/60021



## Abstract

Nitrogen-doped carbon nanocoils (CNCs) with adjusted morphologies were synthesized in a one-step catalytic chemical vapour deposition (CVD) process using acetonitrile as the carbon and nitrogen source. The nickel iron oxide/nickel oxide nanocomposites, which were derived from nickel–iron layered double hydroxide (LDH) precursors, were employed as catalysts for the synthesis of CNCs. In this method, precursor-to-catalyst transformation, catalyst activation, formation of CNCs, and nitrogen doping were all performed in situ in a single process. The morphology (coil diameter, coil pitch, and fibre diameter) and nitrogen content of the synthesized CNCs was individually adjusted by modulation of the catalyst composition and CVD reaction temperature, respectively. The adjustable ranges of the coil diameter, coil pitch, fibre diameter, and nitrogen content were confirmed to be approximately 500±100 nm, 600±100 nm, 100±20 nm, and 1.1±0.3 atom%, respectively.

**Keywords** Carbon Nanocoil, Helical Carbon Nanotube, Coiled Carbon Nanofibre, Catalytic Chemical Vapour Deposition, Layered Double Hydroxide

## 1. Introduction

Carbon nanocoils (CNCs) [1,2], which are also known as helical carbon nanotubes (HCNTs) or coiled carbon nanofibres, have attracted much attention due to their interesting physicochemical properties that originate from their unique three-dimensional structure. CNCs have been exploited in a variety of applications including microwave absorbing materials [3–6], catalyst supports [7–9], electrode materials [10–15], catalysts [16], electrical contact materials [17], and photoconductive materials [18]. In these applications, the performance of CNCs-incorporated products is affected by the morphology of the CNCs (e.g., coil diameter, coil pitch, and fibre diameter), which can vary depend-

ing on the synthesis conditions employed. In general, the synthesis of CNCs is achieved via catalytic chemical vapour deposition (CCVD) processes, which use alloys or metal oxides as catalysts and gaseous hydrocarbons as the carbon source. Control of CNC morphology has been attempted by manipulating synthesis conditions, such as catalyst composition, reaction temperature, hydrocarbon flow rate, and feed gas composition [19–25].

Nitrogen doping of carbon nanofibres has often been performed to enhance their intrinsic properties and functionality. For example, modulation and enhancement of CNC optical [26], electrical [27], and electrochemical properties [28] has been achieved through nitrogen doping. This resulting combination of good performance and versatile functionality of N-doped CNCs renders these materials as promising candidates for use in a range of applications. The control of their morphologies may also be important in ensuring the high performance of N-doped CNCs-incorporated products. However, to the best of our knowledge, there have been no reports on controlling the morphology of N-doped CNCs.

In this study, a fixed-bed CVD process using acetonitrile as both the carbon and nitrogen sources [29] was employed to synthesize N-doped CNCs with adjusted morphologies. $NiFe_2O_4$/NiO nanocomposites derived from Ni–Fe layered double hydroxides (LDHs) were employed as the catalyst. By preparing Ni–Fe LDHs in a mixed-valence Ni(II)–Fe(II)–Fe(III) system, the nickel and iron content was readily adjusted without drastically changing the crystal structure of the catalyst. In the employed CVD system, precursor-to-catalyst transformation, catalyst activation, formation of CNCs, and nitrogen doping advantageously occur *in situ* in a single process [29]. The current study investigates the effect of catalyst composition (Ni/Fe molar ratio) and CVD reaction temperature on the resulting morphology of N-doped CNCs.

## 2. Experimental

### *2.1 Synthesis of Ni–Fe LDHs*

Analytical grade chemicals were used as received without further purification in all of the experiments. Ni(II)–Fe(II)–Fe(III) LDH catalyst precursors with different Ni/Fe molar ratios were synthesized using a modified coprecipitation method [30]. As shown in Table 1, predetermined amounts of nickel(II) chloride hexahydrate ($NiCl_2.6H_2O$), ferrous chloride tetrahydrate ($FeCl_2.4H_2O$), and ferric chloride hexahydrate ($FeCl_3.6H_2O$) were dissolved in 100 mL of deionized and deoxygenated water under a continuous flow of argon at room temperature. All of these prepared solutions contained the same total amount of metal ions (10 mmol) regardless of the Ni/Fe molar ratio. The molar ratio of divalent to trivalent metal ions was also maintained at 4.0:1.0, in which the content of Fe(III) ions was minimized to maintain the hydrotalcite-like structure stabilizing the LDH crystal structure. A 20 mL solution of 1.0 M sodium hydroxide (NaOH) was added dropwise to the solution containing the appropriate metal ions under magnetic stirring to precipitate the desired product. The resulting suspension, which consisted of the metal hydroxides, was allowed to stir for an additional 2 h. Then, the suspension was aged for 24 h at room temperature under static conditions. The resulting dark-green precipitate (i.e., chloride ion-intercalated Ni(II)–Fe(II)–Fe(III) LDH) was washed with deionized water, centrifuged, and decanted. This washing operation was repeated three times, and then the precipitate was dried overnight at 30°C under vacuum.

| Theoretical Ni/Fe ratio | Amount of chlorides [mmol] | | | Actual Ni/Fe ratio in LDH |
|---|---|---|---|---|
| | Ni(II) | Fe(II) | Fe(III) | |
| 0.5 | 3.3 | 4.7 | 2.0 | 0.49 |
| 1.0 | 5.0 | 3.0 | 2.0 | 0.95 |
| 1.5 | 6.0 | 2.0 | 2.0 | 1.47 |
| 2.0 | 6.7 | 1.3 | 2.0 | 1.96 |

**Table 1.** Ni/Fe molar ratio of Ni(II)–Fe(II)–Fe(III) LDHs as catalyst precursors

The Ni/Fe molar ratio in the Ni–Fe LDHs was determined by inductively coupled plasma-optical emission spectrophotometry (ICP-OES; SPS7800, SII NanoTechnology, Japan). The powder X-ray diffraction (XRD) pattern was obtained on an X-ray diffractometer (RINT-1500, Rigaku, Japan; CuK$\alpha$ radiation, 40 kV, 80 mA, $2\theta$=5–70°, scanning rate: 1.0°/min). The $NiFe_2O_4$/NiO nanocomposite catalysts, which were prepared by annealing Ni–Fe LDHs in the CVD system, were also characterized via XRD analysis. The Ni–Fe LDH powder was dried, heated to the CVD reaction temperature under an argon flow, and immediately allowed to cool to room temperature without exposure to acetonitrile vapour. The XRD pattern was measured and the average crystallite size was calculated using Scherrer's formula from the width of the $NiFe_2O_4$ (311) diffraction peak at $2\theta$=35–36°.

### *2.2 Synthesis of CNCs*

N-doped CNCs were synthesized in a fixed-bed CVD process using acetonitrile as both the carbon and nitrogen source. First, the LDH powder (50 mg) was spread onto a copper substrate in a quartz reaction tube (30 mm inner diameter, 1000 mm in length). The quartz tube was horizontally placed in an electric tube furnace coupled with PID temperature control. The LDH powder was dried at 130°C for 2 h under an argon flow. After drying, the furnace temperature was increased at a rate of 30°C/min. Once the desired reaction temperature (750, 800 or 850°C) was reached, acetonitrile vapour, which was produced by bubbling argon through acetonitrile at room temperature, was supplied into the quartz tube. Assuming that the resulting argon gas was saturated with acetonitrile vapour,

the estimated acetonitrile content was determined to be 11.7 vol% (at 25°C). The acetonitrile vapour supply was maintained for 1 h at a constant reaction temperature. Then, the bubbling was terminated, and the furnace was allowed to cool to room temperature. The argon flow rate was held constant at 400 standard cubic centimetres per minute (sccm) throughout the entire process (i.e., from drying to cooling). The pressure in the quartz tube was maintained at atmospheric pressure in all of the experiments. Finally, the copper substrate, with the catalyst, was removed from the quartz tube, and the deposits were characterized. The morphology was imaged by field emission scanning electron microscopy (FE-SEM; JSM-6700F, JEOL, Japan). From the obtained SEM images, the fibre diameter, coil pitch, and coil diameter of 50 coils were averaged for each condition considered. For each SEM image, two or three coils that were clearly visualized were selected for the measurements. The coil diameter was taken as the outer diameter of the CNC. The carbon and nitrogen content in the products was determined based on combustion in oxygen using a CHN elemental analyser (2400 Series II, PerkinElmer, USA). The nitrogen content was calculated using the formula 100N/(C+N), where N and C indicate the atomic percent of nitrogen and carbon, respectively [28]. The composition of nitrogen-containing functional groups was determined by X-ray photoelectron spectroscopy (XPS) using a PHI Quantera II spectrometer (ULVAC-PHI, Japan) equipped with a monochromatic AlK$\alpha$ source (1486.6 eV, 15 kV).

## 3. Results and discussion

Figure 1 shows the SEM images of LDH particles with a Ni/Fe molar ratio of 0.96 before and after annealing at 800°C. Prior to annealing, the LDH particles had a platelet shape with a lateral size of several hundred nanometres. However, the catalyst formed micron-sized aggregates consisting of polyhedral-shaped particles that had a diameter of approximately 1 μm. Similar results were also obtained from samples prepared with different Ni/Fe molar ratios and at different annealing temperatures. Figure 2 shows the XRD patterns of the precursor LDH particles and catalyst particles. The LDH particles exhibited peaks resulting from the LDH crystal planes for all of the Ni/Fe molar ratios. The catalyst particles consisted of $NiFe_2O_4$ and NiO regardless of the Ni/Fe molar ratio and annealing temperature. The NiO content in the catalysts increased as the Ni/Fe molar ratio increased. Figure 3 shows the dependence of the $NiFe_2O_4$ crystallite size on the Ni/Fe molar ratio. The crystallite size was smaller than the particle size, suggesting that the catalyst particles were polycrystalline. As the Ni/Fe molar ratio increased, the crystallite size decreased. The crystal growth of $NiFe_2O_4$ is most likely inhibited by the formation of NiO crystal grains. In contrast, the crystallite size did not exhibit a dependence on the annealing temperature.

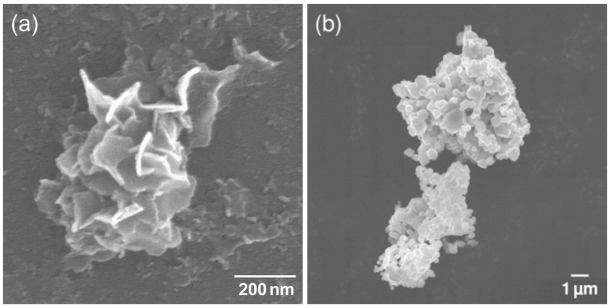


**Figure 1.** SEM images of the (a) Ni–Fe LDH catalyst precursor particles and (b) $NiFe_2O_4$/NiO nanocomposite catalyst particles after annealing at 800°C (Ni/Fe molar ratio = 0.96)

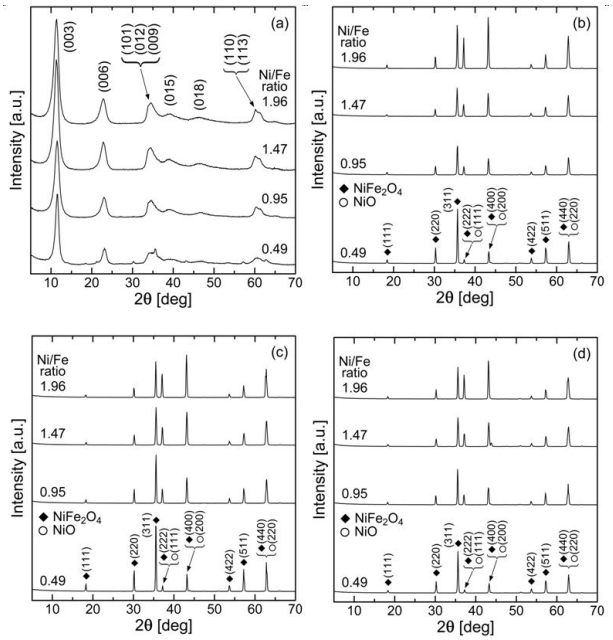


**Figure 2.** XRD patterns of the (a) precursor particles and catalyst particles after annealing at (b) 750°C, (c) 800°C, and (d) 850°C with different Ni/Fe molar ratios

Figure 4 shows a typical SEM image of the CNCs synthesized at 850°C using a catalyst with a Ni/Fe molar ratio of 1.47. We confirmed that the CNCs most likely had hollow, tube-like structures and the quality of the CNCs in the products was nearly the same regardless of the conditions. A similar concentration of coiled fibres formed irrespective of the catalyst composition and reaction temperature. However, the morphology varied depending on the growth conditions. Figure 5 shows the variation in coil diameter, coil pitch, and fibre diameter with an increasing Ni/Fe molar ratio as well as reaction temperature. The plots and vertical error bars represent the mean value and standard deviation of the mean value for each condition considered, respectively. The coil diameter, coil pitch, and fibre diameter decreased with increasing Ni/Fe molar ratio. The coil diameter and coil pitch exhibited little dependence on the reaction temperature. However, the fibre diameter tended to slightly decrease at higher temperatures, sug-

gesting a decrease in the solubility of carbon in the catalysts at higher temperatures [24].

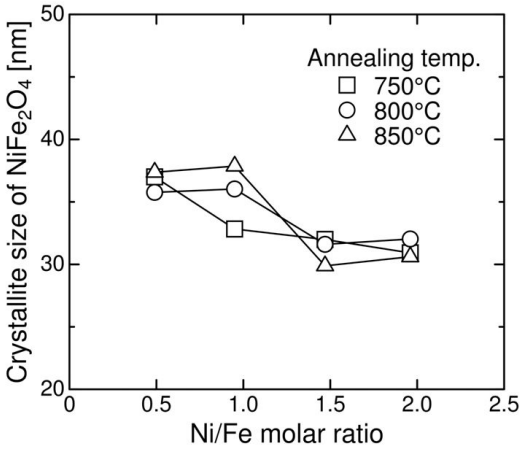


**Figure 3.** Variation in the crystallite size of $NiFe_2O_4$ in the catalyst particles with increasing Ni/Fe molar ratio and annealing temperature

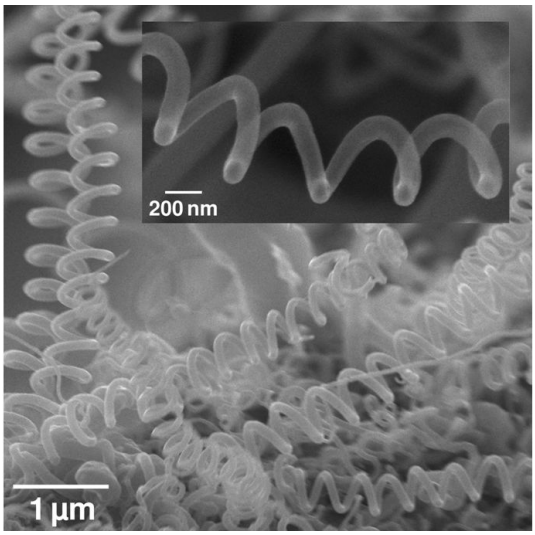


**Figure 4.** SEM image of the CNC product obtained at a reaction temperature of 850°C using a catalyst with a Ni/Fe molar ratio of 1.47

The growth of CNCs can be affected not only by $NiFe_2O_4$ but also by NiO in the catalyst. The NiO crystallite size can increase with an increasing Ni/Fe molar ratio. However, as shown in Figures 3 and 5, the $NiFe_2O_4$ crystallite size and CNC morphology had a similar tendency to vary depending on the conditions. Therefore, the effect of the NiO crystallite on the morphology in this synthesis process may be relatively small compared to that of $NiFe_2O_4$.

There is no clear dependence of the quality of the CNCs on temperature due to a relatively small temperature difference [31] even though the yield was dependent on both the catalyst composition and temperature, as shown in Figure 6. It is well known that the catalyst composition plays a critical role in determining CNC morphology [19,20,22,23]. In particular, the carbon deposition rate correlates strongly with the constituent element in the catalysts. The appropriate combinations of the constituent elements allow for the preparation of helical carbon fibres. Therefore, it is believed that fine CNCs were obtained at higher Ni/Fe molar ratios because an increasing iron content favours higher carbon deposition rates compared to nickel (Figure 6). However, this behaviour may also be due to the smaller crystallite size of the catalysts that are obtained at higher Ni/Fe molar ratios (Figure 3). The adjustable ranges of the coil diameter, coil pitch, and fibre diameter were determined to be approximately 400–600 nm, 500–700 nm, and 80–120 nm, respectively.

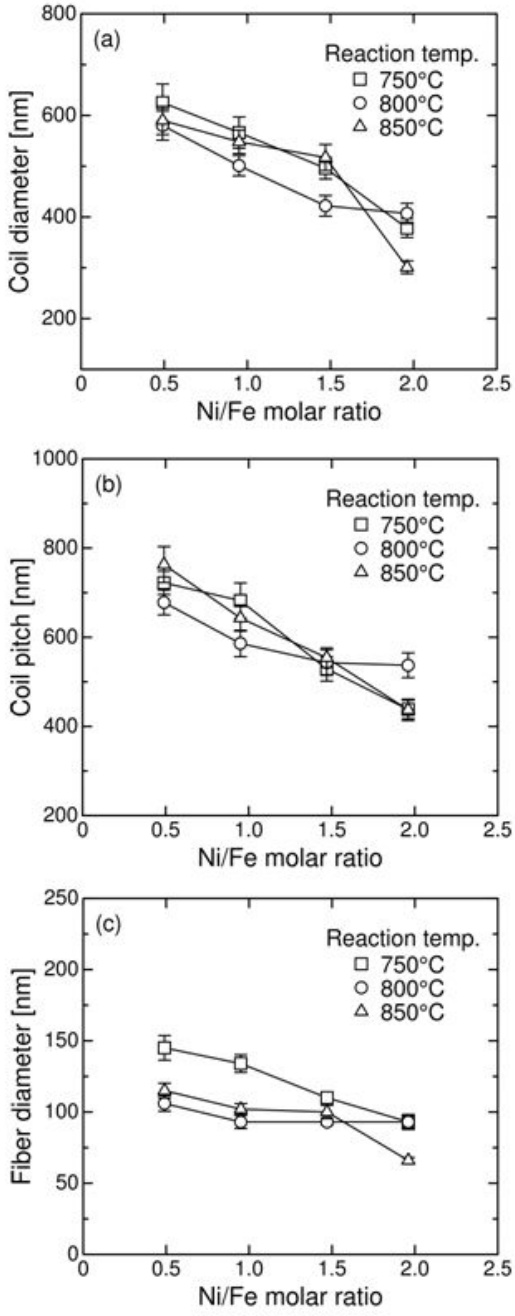


**Figure 5.** Effect of the catalyst Ni/Fe molar ratio and reaction temperature on the (a) coil diameter, (b) coil pitch, and (c) fibre diameter of the CNC products

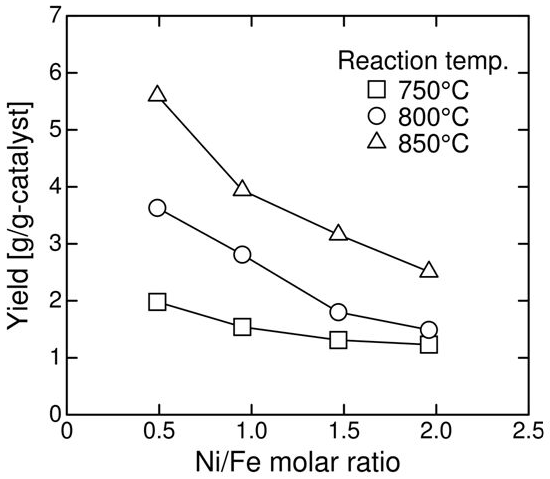


**Figure 6.** Effect of the catalyst Ni/Fe molar ratio and reaction temperature on the product yield

Figure 7 shows the nitrogen content of the products as a function of the reaction temperature. The nitrogen content was determined to decrease as the reaction temperature increased. In contrast, the Ni/Fe molar ratio exhibited little effect on the resulting nitrogen content. These results suggest that the nitrogen content and morphology of the N-doped CNCs can be adjusted by individual manipulation of the reaction temperature and catalyst composition. The obtained nitrogen content was within the range of 0.8–1.4 atom%, which was equivalent to or exceeded that achieved from conventional methods [32]. A typical XPS N1s spectrum is shown in Figure 8. The spectrum was fitted to three Gaussian-type components located at approximately 398.5, 401.1, and 404.4 eV, which correspond to pyridinic nitrogen, graphitic nitrogen, and molecular nitrogen, respectively [33]. The content ratio of different nitrogen forms was estimated using integrated peak areas to be pyridinic/graphitic=36.2/63.8, which was close to that obtained in the synthesis of N-doped CNTs using acetonitrile as the nitrogen source [34,35].

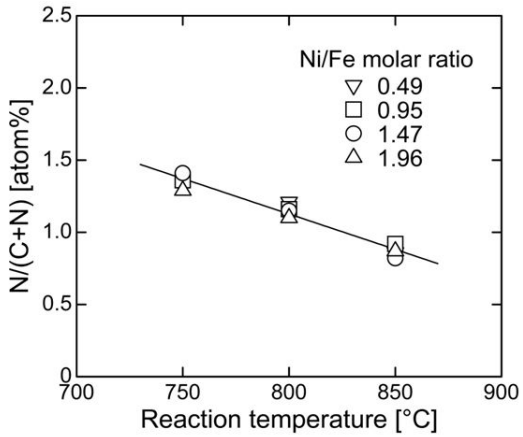


**Figure 7.** Effect of the reaction temperature and catalyst Ni/Fe molar ratio on the nitrogen content in the products

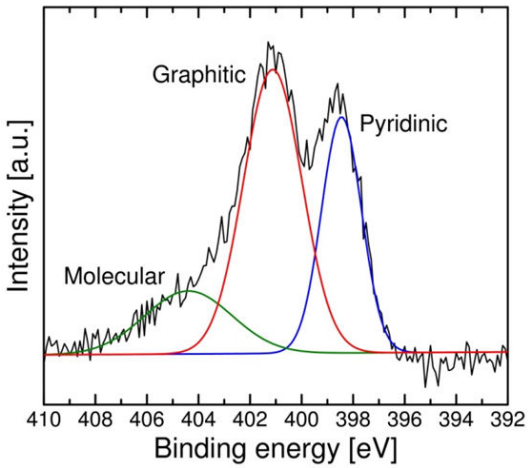


**Figure 8.** XPS N1s spectrum of the product obtained at a reaction temperature of 750°C using a catalyst with a Ni/Fe molar ratio of 1.47

## 4. Conclusions

Using a one-step CCVD process employing Ni–Fe LDHs and acetonitrile as a catalyst precursor and carbon/nitrogen source, respectively, we demonstrated adjustment of the morphology and nitrogen content of N-doped CNCs. The coil diameter, coil pitch, and fibre diameter of the nanostructures decreased as the Ni/Fe molar ratio of the employed catalysts increased. In addition, the nitrogen content of the CNCs was determined to increase as the reaction temperature decreased. The obtained results suggest that the morphology and nitrogen content can be individually adjusted by manipulation of the Ni/Fe molar ratio and the reaction temperature, respectively. The nitrogen on the CNCs can be expected to act as anchoring sites for catalyst metal nanoparticle deposition [27]. In the future, the adjustable ranges of coil diameter, coil pitch, fibre diameter, and nitrogen content need to be further extended.

## 5. Acknowledgements

This work was financially supported in part by JSPS KAKENHI grant number 26289298.

## 6. References

[1] Ivanov V, Nagy JB, Lambin Ph, Lucas A, Zhang XB, Zhang XF, Bernaerts D, Van Tendeloo G, Amelinckx S, Van Landuyt J (1994) The study of carbon nanotubules produced by catalytic method. Chem. Phys. Lett. 223: 329–335.

[2] Hanus MJ, Harris AT (2010) Synthesis, characterisation and applications of coiled carbon nanotubes. J. Nanosci. Nanotechnol. 10: 2261–2283.

[3] Tang N, Yang Y, Lin K, Zhong W, Au C, Du Y (2008) Synthesis of plait-like carbon nanocoils in ultrahigh yield, and their microwave absorption properties. J. Phys. Chem. C 112: 10061–10067.

[4] Tang N, Zhong W, Au C, Yang Y, Han M, Lin K, Du Y (2008) Synthesis, microwave electromagnetic, and microwave absorption properties of twin carbon nanocoils. J. Phys. Chem. C 112: 19316–19323.

[5] Zhao DL, Shen ZM (2008) Preparation and microwave absorption properties of carbon nanocoils. Mater. Lett. 62: 3704–3706.

[6] Qi X, Yang Y, Zhong W, Deng Y, Au C, Du Y (2009) Large-scale synthesis, characterization and microwave absorption properties of carbon nanotubes of different helicities. J. Solid State Chem. 182: 2691–2697.

[7] Hu G, Nitze F, Barzegar HR, Sharifi T, Mikołajczuk A, Tai CW, Borodzinski A, Wågberg T (2012) Palladium nanocrystals supported on helical carbon nanofibers for highly efficient electrooxidation of formic acid, methanol and ethanol in alkaline electrolytes. J. Power Sources 209: 236–242.

[8] Hu G, Nitze F, Sharifi T, Barzegar HR, Wågberg T (2012) Self-assembled palladium nanocrystals on helical carbon nanofibers as enhanced electrocatalysts for electro-oxidation of small molecules. J. Mater. Chem. 22: 8541–8548.

[9] Nitze F, Mazurkiewicz M, Malolepszy A, Mikolajczuk A, Kędzierzawski P, Tai CW, Hu G, Kurzydłowski KJ, Stobinski L, Borodzinski A, Wågberg T (2012) Synthesis of palladium nanoparticles decorated helical carbon nanofiber as highly active anodic catalyst for direct formic acid fuel cells. Electrochim. Acta 63: 323–328.

[10] Wang L, Li C, Gu F, Zhang C (2009) Facile flame synthesis and electrochemical properties of carbon nanocoils. J. Alloys Compd. 473: 351–355.

[11] Rakhi RB, Cha D, Chen W, Alshareef HN (2011) Electrochemical energy storage devices using electrodes incorporating carbon nanocoils and metal oxides nanoparticles. J. Phys. Chem. C 115: 14392–14399.

[12] Cui R, Han Z, Pan J, Abdel-Halim ES, Zhu JJ (2011) Direct electrochemistry of glucose oxidase and biosensing for glucose based on helical carbon nanotubes modified magnetic electrodes. Electrochim. Acta 58: 179–183.

[13] Cui R, Wang X, Zhang G, Wang C (2012) Simultaneous determination of dopamine, ascorbic acid, and uric acid using helical carbon nanotubes modified electrode. Sensor Actuat. B Chem. 161: 1139–1143.

[14] Rakhi RB, Chen W, Alshareef HN (2012) Conducting polymer/carbon nanocoil composite electrodes for efficient supercapacitors. J. Mater. Chem. 22: 5177–5183.

[15] Barranco V, Celorrio V, Lazaro MJ, Rojo JM (2012) Carbon nanocoils as unusual electrode materials for supercapacitors batteries and energy storage. J. Electrochem. Soc. 159: A464–A469.

[16] Cui R, Han Z, Zhu JJ (2011) Helical carbon nanotubes: intrinsic peroxidase catalytic activity and its application for biocatalysis and biosensing. Chem.-Eur. J. 17: 9377–9384.

[17] Tang N, Kuo W, Jeng C, Wang L, Lin K, Du Y (2010) Coil-in-coil carbon nanocoils: 11 gram-scale synthesis, single nanocoil electrical properties, and electrical contact improvement. ACS Nano 4: 781–788.

[18] Liu Y, Tang N, Kuo W, Jiang C, Wen J, Du Y (2012) N-doped helical carbon nanotubes: single helix photoconductivity and photoluminescence properties. J. Phys. Chem. C 116: 14584–14590.

[19] Ren X, Zhang H, Cui Z (2007) Acetylene decomposition to helical carbon nanofibers over supported copper catalysts. Mater. Res. Bull. 42: 2202–2210.

[20] Yokota M, Hosokawa Y, Shinohara Y, Kawabata T, Takimoto K, Suda Y, Oke S, Takikawa H, Fujimura Y, Yamaura T, Itoh S, Ue H, Morioki M (2010) Splitting and flattening of helical carbon nanofibers by acid treatment. J. Nanosci. Nanotechnol. 10: 3910–3914.

[21] Yokota M, Suda Y, Takikawa H, Ue H, Shimizu K, Umeda Y (2011) Structural analysis of multi-walled carbon nanocoils synthesized with Fe-Sn catalyst supported on zeolite. J. Nanosci. Nanotechnol. 11: 2344–2348.

[22] Csató A, Szabó A, Fonseca A, Vuono D, Kónya Z, Volodin A, Van Haesendonck C, Biro LP, Giordano G, Nagy JB (2012) Synthesis and characterisation of coiled carbon nanotubes. Catal. Today 181: 33–39.

[23] Qi X, Zhong W, Yao X, Zhang H, Ding Q, Wu Q, Deng Y, Au C, Du Y (2012) Controllable and large-scale synthesis of metal-free carbon nanofibers and carbon nanocoils over water-soluble $Na_xK_y$ catalysts. Carbon 50: 646–658.

[24] Li D, Pan L, Wu Y, Peng W (2012) The effect of changes in synthesis temperature and acetylene supply on the morphology of carbon nanocoils. Carbon 50: 2571–2580.

[25] Li X, Xu Z (2012) Controllable synthesis of helical, straight, hollow and nitrogen-doped carbon nanofibers and their magnetic properties. Mater. Res. Bull. 47: 4383–4391.

[26] Wen J, Zhang Y, Tang N, Wan X, Xiong Z, Zhong W, Wang Z, Wu X, Du Y (2011) Synthesis, photoluminescence, and magnetic properties of nitrogen-doping helical carbon nanotubes. J. Phys. Chem. C 115: 12329–12334.

[27] Jafri RI, Rajalakshmi N, Ramaprabhu S (2010) Nitrogen-doped multi-walled carbon nanocoils as catalyst support for oxygen reduction reaction in proton exchange membrane fuel cell. J. Power Sources 195: 8080–8083.

[28] Cao B, Zhang B, Jiang X, Zhang Y, Pan C (2011) Direct synthesis of high concentration N-doped

coiled carbon nanofibers from amine flames and its electrochemical properties. J. Power Sources 196: 7868–7873.

[29] Iwasaki T, Tomisawa M, Nakamura H, Watano S (2013) Synthesis of nitrogen-doped carbon nanocoils via one-step acetonitrile catalytic CVD using a Ni-Fe layered double hydroxide as catalyst precursor. Chem. Vap. Depos. 19: 323–326.

[30] Chaves LHG, Curry JE, Stone DA, Carducci MD, Chorover J (2009) Nickel incorporation in Fe(II, III) hydroxysulfate Green Rust: effect on crystal lattice spacing and oxidation products. Rev. Bras. Ciênc. Solo 33: 1115–1123.

[31] Nitze F, Abou-Hamad E, Wågberg T (2011) Carbon nanotubes and helical carbon nanofibers grown by chemical vapour deposition on $C_{60}$ fullerene supported Pd nanoparticles. Carbon 49: 1101–1107.

[32] Bulusheva LG, Okotrub AV, Kudashov AG, Shubin YV, Shlyakhova EV, Yudanov NF, Pazhetnov EM, Boronin AI, Vyalikh DV (2008) Effect of Fe/Ni catalyst composition on nitrogen doping and field emission properties of carbon nanotubes. Carbon 46: 864–869.

[33] Ibrahim EMM, Khavrus VO, Leonhardt A, Hampel S, Oswald S, Rümmeli MH, Büchner B (2010) Synthesis, characterization, and electrical properties of nitrogen-doped single-walled carbon nanotubes with different nitrogen content. Diam. Relat. Mater. 19: 1199–1206.

[34] Bulusheva LG, Okotrub AV, Kurenya AG, Zhang H, Zhang H, Chen X, Song H (2011) Electrochemical properties of nitrogen-doped carbon nanotube anode in Li-ion batteries. Carbon 49: 4013–4023.

[35] Liu J, Zhang Y, Ionescu MI, Li R, Sun X (2011) Nitrogen-doped carbon nanotubes with tunable structure and high yield produced by ultrasonic spray pyrolysis. Appl. Surf. Sci. 257: 7837–7844.